A Series-Connected 24-Pulse Rectifier Using Passive Voltage Harmonic Injection Method at DC-Link

Fangang Meng, *Member, IEEE*, Qingxiao Du, Lin Wang, Lei Gao, and Zhongcheng Man

***Abstract*—In this paper, a voltage harmonic injection method at the dc-link is proposed to reduce input current harmonics of the series-connected 12-pulse rectifier. The proposed method uses an auxiliary circuit to generate the voltage harmonics and injects the voltage harmonics into the dc link of the series-connected 12-pulse rectifier so that the input voltages of the 12-pulse rectifier can be shaped as 24 steps. The formation processes of the input voltage are analyzed based on the switching functions; and the turn ratio of injection transformer is optimally designed from the perspective of minimizing the total harmonic distortion (THD) of the input voltage. After using this method, experimental results show that the input voltages of the isolated transformer are 24-step waves with an experimental THD of around 3.34%; the input line currents of the proposed rectifier are close to sinusoidal waveforms with an experimental THD of around 2.65%. More importantly, the kVA rating of the injection transformer is only about 2.3% of the load power, which means that the cost of harmonicreduction is very low.**

***Index Terms*—Harmonic injection, injection transformer, passive harmonic reduction, series-connected multi-pulse rectifier.**

I. Introduction

MULTI-PULSE diode-bridge rectifier with properties of a simple structure and strong robustness has been widely used in high-power rectifications. However, due to the nonlinearity of the diode-bridge rectifier, the multi-pulse rectifier generates a large number of harmonics injected into the grids; for example, the total harmonic distortion (THD) of the input line current in the 12-pulse rectifier is up to 15.2%, which cannot be ignored [1]. Therefore, how to improve the harmonic reduction ability and power factor of the multi-pulse diode-bridge rectifier has become an important topic in the field of high-power rectification.

In general, a multipulse rectifier comprises a phase-shifting transformer and two or more three-phase diode-bridge rectifiers, which can be divided into parallel and series types based on the connection methods of the diode-bridge rectifiers [2]. When

Manuscript received July 31, 2018; revised October 20, 2018; accepted December 20, 2018. Date of publication December 24, 2018; date of current version June 10, 2019. This work was supported in part by the National Natural Foundation of China under Grants 51777042 and 51677016, by the China Postdoctoral Science Foundation under Grants 2016M590281 and 2017T100241. Recommended for publication by Associate Editor J.-I. Itoh. *(Corresponding author: Lei Gao.)*

The authors are with the School of Electrical Engineering and Automation, Harbin Institute of Technology, Harbin 150006, China (e-mail:

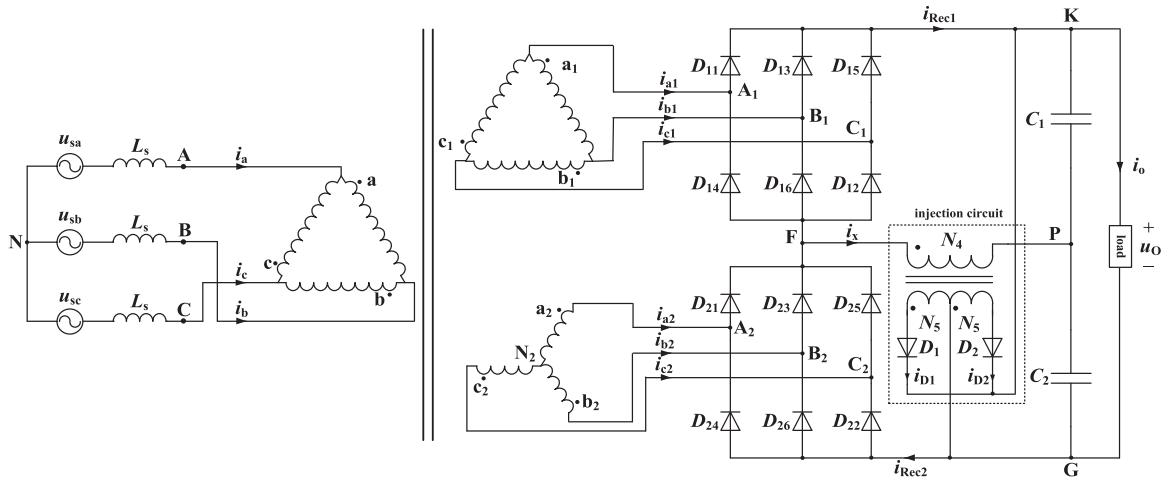

Fig. 1. Proposed series-connected 24-pulse rectifier with a passive voltage harmonic injection method at dc-link.

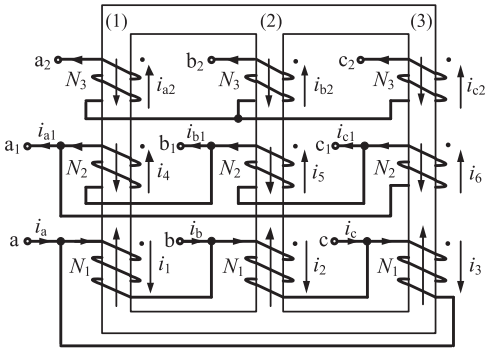

Fig. 2. Winding configuration of the $\Delta/\Delta/Y$ isolated transformer.

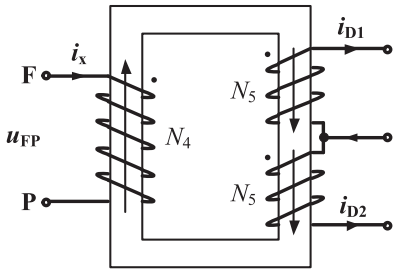

Fig. 3. Winding configuration of injection transformer.

so that the proposed rectifier can be equivalent to a current source converter. At the dc-link, two large capacitors C_1 and C_2 are used, thus the ripple of the load voltage is quite small, and the load can be equal to a constant-voltage load. A $\Delta/\Delta/Y$ isolated transformer is used to be the phase-shifting transformer, and Fig. 2 shows its winding configuration. In Fig. 2, the phase-shifting can output two sets of three-phase voltages with $\pi/6$ phase difference, and the turn ratio of the phase-shifting transformer meets that $N_1 : N_2 : N_3 = \sqrt{3} : \sqrt{3} : 1$.

The harmonic injection circuit consists of an injection transformer and a single-phase diode rectifier. The winding configuration of the injection transformer is shown in Fig. 3. The primary winding of the injection transformer is connected between the midpoint of the two series-connected three-phase bridge rectifiers and the midpoint of the output capacitance, and the secondary winding has a center tap. The input terminal of the single-phase diode rectifier is connected with the secondary winding of the injection transformer, and the output terminal is connected with the load.

III. Operation of the Proposed 24-Pulse Rectifier

The series-connected 12-pulse rectifier can be equivalent to a current source converter with constant-voltage load, so the input voltages of the phase-shifting transformer depend on the load voltage. In this section, operating modes of the harmonic injection circuits are clearly illustrated at first, then some optimal design processes of the injection transformer are described based on the objective of minimizing the THD of the phase-shifting transformer's input voltage.

A. Operation Modes of the Harmonic Injection Circuit

Because the series-connected 12-pulse rectifier can be viewed as a current source converter, the two three-phase bridge rectifiers can be replaced by two current sources (i_{Rec1} and i_{Rec2}), which provide 6-pulse currents with $\pi/6$ phase differences. In addition, the harmonic injection circuit can generate voltage harmonics at the dc-link due to the existence of the phase difference between i_{Rec1} and i_{Rec2}. According to the phase relation between i_{Rec1} and i_{Rec2}, it can be concluded that the harmonic injection circuit has two operating modes, as shown in Fig. 4.

1) Operating Mode I: When $i_{\mathrm{Rec1}}<i_{\mathrm{Rec2}}$, the harmonic injection circuit operates at the operating mode I, as shown in Fig. 4(a). Under this mode, i_x is greater than zero, the diode D_1 is forward-biased and turns ON, while the diode D_2 is reverse-biased and turns OFF.

Assume that the load voltage is u_o, and the forward conduction voltage drop of the diodes D_1 and D_2 is U_d. From Fig. 4(a), the voltage across the primary winding voltage of the injection transformer can be expressed as

$$u_{\mathrm{FP}} = \frac{N_4}{N_5}\left(u_o + U_d\right) \tag{1}$$

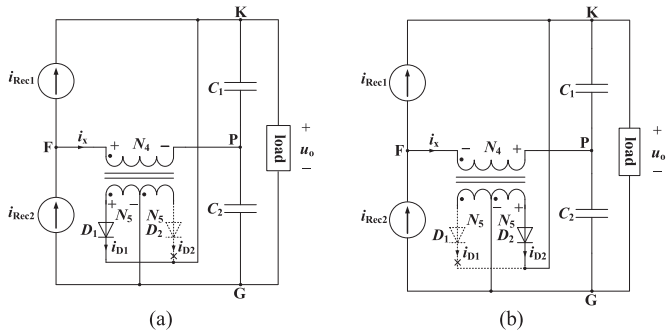

Fig. 4. Operating mode of harmonic injection circuit. (a) Operating mode I. (b) Operating mode II.

where N_4 and N_5 are the turn numbers of the primary and secondary windings of the injection transformer, respectively; u_o is the load voltage.

2) Operating Mode II: When $i_{\mathrm{Rec1}}>i_{\mathrm{Rec2}}$, the harmonic injection circuit operates at the operating mode II, as shown in Fig. 4(b). Under this mode, i_x is less than zero, the diode D_2 is forward-biased and turns ON, and the diode D_1 is reverse-biased and turns OFF. From Fig. 4(b), the voltage across the primary winding voltage of the injection transformer can be expressed as

$$u_{\mathrm{FP}} = -\frac{N_4}{N_5}\left(u_o + U_d\right). \tag{2}$$

In order to facilitate the analysis, u_x is defined as below

$$u_x = \frac{N_4}{N_5}\left(u_o + U_d\right). \tag{3}$$

From (1) and (2), the harmonic injection circuit can generate a square wave voltage with an amplitude of $\pm u_x$, and the frequency of the square wave voltage is six times of the supply frequency.

B. 24-Step Wave Formation Process

From the winding configuration of the phase-shifting transformer, the relation between its input voltage and the voltage across its secondary winding can be expressed as

$$u_{\mathrm{AN}} = \frac{1}{\sqrt{3}} u_{A1B1} \angle -\frac{\pi}{6} \tag{4}$$

where u_{AN} is the input voltage of the phase-shifting transformer and u_{A1B1} is the voltage across its secondary winding.

From (4), the input voltage can be obtained by calculating the voltage across the secondary winding.

In order to facilitate the analysis, define switching function of the injection transformer as $S_x(\omega t) = \mathrm{sgn}(u_{\mathrm{FP}})$, and sgn($x$) is a symbolic function defined as follows:

$$\mathrm{sgn}(x) \triangleq \begin{cases} 1 & x > 0 \\ 0 & x = 0 \\ -1 & x < 0. \end{cases} \tag{5}$$

From the operating mode of the injection transformer, the switching function S_x can be expressed as

$$S_x = \begin{cases} 1 & \omega t \in \left[\phi + \frac{\pi}{12} + \frac{k\pi}{3}, \phi + \frac{\pi}{4} + \frac{k\pi}{3}\right) \\ -1 & \omega t \in \left[\phi + \frac{\pi}{4} + \frac{k\pi}{3}, \phi + \frac{5\pi}{12} + \frac{k\pi}{3}\right] \end{cases} \tag{6}$$

where *k* is the natural number.

Define the switching functions of phase a1, b1, c1, a2, b2, and c2 as S_{a1}, S_{b1}, S_{c1}, S_{a2}, S_{b2}, and S_{c2}, respectively. These switching functions can be obtained from the following analysis.

Assuming that the input voltage of the rectifier are balanced

$$\begin{cases} u_{sa} = \sqrt{2}U_s \sin(\omega t) \\ u_{sb} = \sqrt{2}U_s \sin(\omega t - 2\pi/3) \\ u_{sc} = \sqrt{2}U_s \sin(\omega t + 2\pi/3) \end{cases} \tag{7}$$

where U_s is the rms of the input voltage.

Since the input inductance L_s is connected in series with the ac voltage source, there is a phase difference ϕ between the input voltage of Δ/Δ/Y isolated transformer and the ac voltage source. Accordingly, the input voltage of the Δ/Δ/Y isolated transformer can be approximately represented by the fundamental voltage

$$\begin{cases} u_{\mathrm{AN}} \approx U_{s1} \sin(\omega t - \phi) \\ u_{\mathrm{BN}} \approx U_{s1} \sin\left(\omega t - \frac{2}{3}\pi - \phi\right) \\ u_{\mathrm{CN}} \approx U_{s1} \sin\left(\omega t + \frac{2}{3}\pi - \phi\right) \end{cases} \tag{8}$$

where U_{s1} is the fundamental voltage amplitude of the input voltage of isolation transformer.

From (8), the output voltage of the Δ/Δ/Y isolated transformer can be expressed as

$$\begin{cases} u_{a1} \approx U_1 \sin(\omega t - \phi) \\ u_{b1} \approx U_1 \sin\left(\omega t - \frac{2}{3}\pi - \phi\right) \\ u_{c1} \approx U_1 \sin\left(\omega t + \frac{2}{3}\pi - \phi\right) \end{cases} \quad \begin{cases} u_{a2} \approx U_1 \sin\left(\omega t + \frac{\pi}{6} - \phi\right) \\ u_{b2} \approx U_1 \sin\left(\omega t - \frac{\pi}{2} - \phi\right) \\ u_{c2} \approx U_1 \sin\left(\omega t + \frac{5}{6}\pi - \phi\right). \end{cases} \tag{9}$$

The output voltages of the Δ/Δ/Y isolated transformer determine the switching functions. From (9) and Fig. 1, the switching function S_{a1} is calculated as

$$S_{a1} = \begin{cases} 0 & \omega t \in [\phi - \frac{\pi}{6} + 2k\pi, \phi + \frac{\pi}{6} + 2k\pi) \\ 1 & \omega t \in [\phi + \frac{\pi}{6} + 2k\pi, \phi + \frac{5\pi}{6} + 2k\pi) \\ 0 & \omega t \in [\phi + \frac{5\pi}{6} + 2k\pi, \phi + \frac{7\pi}{6} + 2k\pi) \\ -1 & \omega t \in [\phi + \frac{7\pi}{6} + 2k\pi, \phi + \frac{11\pi}{6} + 2k\pi]. \end{cases} \tag{10}$$

The relation among the switching functions meets

$$\begin{cases} S_{b1} = S_{a1} \angle -\frac{2}{3}\pi \\ S_{c1} = S_{a1} \angle \frac{2}{3}\pi \end{cases} \quad \begin{cases} S_{a2} = S_{a1} \angle \frac{\pi}{6} \\ S_{b2} = S_{a1} \angle -\frac{\pi}{2} \\ S_{c2} = S_{a1} \angle \frac{5}{6}\pi. \end{cases} \tag{11}$$

From (6), (10), and (11), in one power supply cycle, the switching functions S_x, S_{a1}, S_{b1}, S_{c1}, S_{a2}, S_{b2}, and S_{c2} have 24 combinations. For the sake of simplicity, only one combination is analyzed, and assumes that the switching function satisfies

the following condition:

$$\begin{cases} S_{a1}=0,\ S_{b1}=-1\ ,\ S_{c1}=1 \\ S_{a2}=1,\ S_{b2}=-1\ ,\ S_{c2}=0 \\ S_x=-1. \end{cases} \tag{12}$$

From (12) and Fig. 1, the voltages $u_{B1P}, u_{C1P}, u_{A2G}, u_{B2G}$ can be expressed as

$$\begin{cases} u_{B1P}=-u_x-U_d \\ u_{C1P}=\frac{u_o}{2}+U_d \end{cases} \quad \begin{cases} u_{A2G}=\frac{u_o}{2}-u_x+U_d \\ u_{B2G}=-U_d. \end{cases} \tag{13}$$

As shown in Figs. 1 and 2, the voltages across the star-connected secondary windings meet

$$\begin{cases} u_{A2N2}=u_{A2G}-u_{N2G} \\ u_{B2N2}=u_{B2G}-u_{N2G} \\ u_{C2N2}=u_{C2G}-u_{N2G} \\ u_{A2N2}+u_{B2N2}+u_{C2N2}=0. \end{cases} \tag{14}$$

From (14), u_{N2G} can be calculated as

$$u_{N2G}=\frac{u_{A2G}+u_{B2G}+u_{C2G}}{3}. \tag{15}$$

From (13), (14), and (15), u_{N2G}, u_{A2N2}, and u_{B2N2} can be written as

$$\begin{cases} u_{N2G}=\frac{1}{3}\left(\frac{u_o}{2}-u_x+u_{C2G}\right) \\ u_{A2N2}=\frac{2}{3}\left(\frac{u_o}{2}-u_x\right)-\frac{1}{3}u_{C2G}+U_d \\ u_{B2N2}=-\frac{1}{3}\left(\frac{u_o}{2}-u_x+u_{C2G}\right)-U_d. \end{cases} \tag{16}$$

On the basis of (12), expressions of u_{A1B1} and u_{B1C1} are given as follows:

$$\begin{cases} u_{A1B1}=u_{A1P}-u_{B1P}=u_{A1P}+u_x+U_d \\ u_{B1C1}=u_{B1P}-u_{C1P}=-\frac{u_o}{2}-u_x-2U_d. \end{cases} \tag{17}$$

According to the turn ratio of the Δ/Δ/Y isolated transformer, the relationship between the primary winding voltage and the secondary winding voltage of the isolation transformer satisfies the following relation:

$$\begin{cases} u_{A1B1}=u_{\mathrm{AB}}=\sqrt{3}u_{A2N2} \\ u_{B1C1}=u_{\mathrm{BC}}=\sqrt{3}u_{B2N2}. \end{cases} \tag{18}$$

Substituting (16) and (17) in (18), u_{A1P} and u_{C2G} can be expressed as

$$\begin{cases} u_{A1P}=\dfrac{\sqrt{3}-1}{2}u_o-(2+\sqrt{3})u_x+(2\sqrt{3}-3)U_d \\ u_{C2G}=\dfrac{\sqrt{3}-1}{2}u_o+(\sqrt{3}+1)u_x+(2\sqrt{3}-3)U_d. \end{cases} \tag{19}$$

According to (19) and (17), the voltage u_{A1B1} in this combination is calculated as

$$u_{A1B1}=\frac{\sqrt{3}-1}{2}(u_o+4U_d)-(\sqrt{3}+1)u_x. \tag{20}$$

Substituting (3) and (20) in (4) yields

$$u_{\mathrm{AN}}=\frac{\sqrt{3}-1}{2\sqrt{3}}(u_o+4U_d)-\frac{(\sqrt{3}+1)N_4}{\sqrt{3}N_5}(u_o+U_d). \tag{21}$$

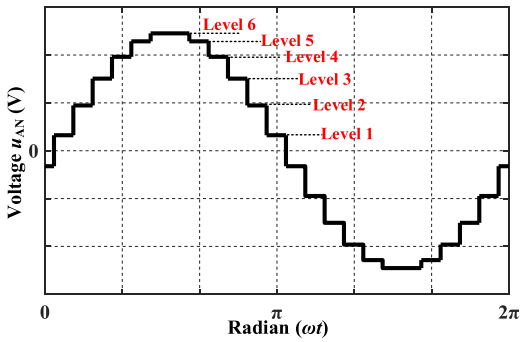

Fig. 5. Input voltage u_{AN} of isolation transformer.

TABLE I
LEVELS OF THE VOLTAGE u_{AN}

voltage	level
$u_{\text{AN-level1}}$	$\frac{2-\sqrt{3}}{2\sqrt{3}}(u_o+4U_d)-\frac{(2+\sqrt{3})N_4}{\sqrt{3}N_5}(u_o+U_d)$
$u_{\text{AN-level2}}$	$\frac{2-\sqrt{3}}{2\sqrt{3}}(u_o+4U_d)+\frac{(2+\sqrt{3})N_4}{\sqrt{3}N_5}(u_o+U_d)$
$u_{\text{AN-level3}}$	$\frac{\sqrt{3}-1}{2\sqrt{3}}(u_o+4U_d)-\frac{(\sqrt{3}+1)N_4}{\sqrt{3}N_5}(u_o+U_d)$
$u_{\text{AN-level4}}$	$\frac{\sqrt{3}-1}{2\sqrt{3}}(u_o+4U_d)+\frac{(\sqrt{3}+1)N_4}{\sqrt{3}N_5}(u_o+U_d)$
$u_{\text{AN-level5}}$	$\frac{1}{2\sqrt{3}}(u_o+4U_d)-\frac{N_4}{\sqrt{3}N_5}(u_o+U_d)$
$u_{\text{AN-level6}}$	$\frac{1}{2\sqrt{3}}(u_o+4U_d)+\frac{N_4}{\sqrt{3}N_5}(u_o+U_d)$

Similarly, the expressions of u_{AN} in the other 23 combinations can be obtained. Fig. 5 shows the theoretical waveform of u_{AN}, and Table I gives the level values for each step of u_{AN}.

C. Optimum Turn Ratio Design of Injection Transformer

In order to ensure that the proposed rectifier operates as a 24-pulse rectifier, it is necessary to optimize the turn ratio of the injection transformer from the viewpoint of minimizing the THD of the input voltages (u_{An1}, u_{Bn1}, u_{Cn1}).

In Fig. 3, assume that the ratio of N_5 to N_4 is equal to n. From Fig. 5 and Table I

$$\begin{cases} U_{\mathrm{AN}}=\sqrt{\frac{1}{3}\left[\frac{2-\sqrt{3}}{2}(u_o+4U_d)^2+2(2+\sqrt{3})\left(\frac{u_o+U_d}{n}\right)^2\right]} \\ U_{s1}=-\frac{4\sqrt{3}}{\pi}\left[\frac{\sqrt{3}-2}{2}(u_o+4U_d)+\frac{\sqrt{2}-\sqrt{3}}{\sqrt{2}+1}\frac{u_o+U_d}{n}\right] \end{cases} \tag{22}$$

where U_{AN} and U_{s1} are the rms value and fundamental voltage amplitude of u_{AN}, respectively.

Define the THD of the input voltage u_{AN} as

$$\mathrm{THD}=\frac{\sqrt{2U_{\mathrm{AN}}^2-U_{s1}^2}}{U_{s1}}. \tag{23}$$

Substituting (22) into (23), the relation between the THD of the input voltage u_{AN} and the turn ratio n can be obtained, as

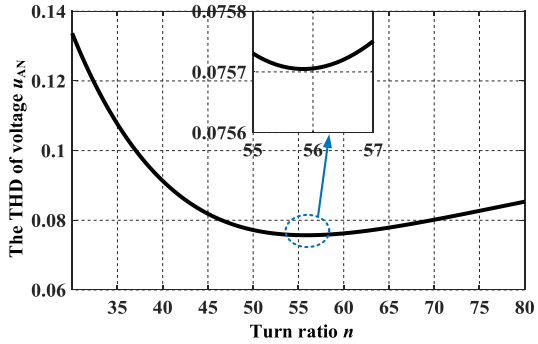

Fig. 6. Relation between the THD and turn ratio n.

shown in Fig. 6. It can be easily seen from Fig. 6 that when n (N_5/N_4) is around 55.8, the corresponding minimum THD value is about 7.57%. Therefore, when the injection transformer operates as a step-up transformer and $N_5 >> N_4$, the diodes D_1 and D_2 conduct in turn to generate the voltage harmonic and inject the voltage harmonics into the dc-link of the proposed rectifier.

D. Input Line Current of the Proposed Rectifier

In Fig. 1, the voltage across inductor L_s can be expressed as

$$u_{Ls} = L_s \frac{di_a}{dt} = u_{sa} - u_{An1}. \tag{24}$$

For the sake of analysis, the voltages and currents are normalized. When the voltages are normalized, the amplitude of the input voltage U_s is viewed as the reference value. The voltages u_{Ls}, u_{sa}, u_{An1}, u_o, and U_d are expressed as

$$\begin{cases} u_{mLs} = \dfrac{u_{Ls}}{U_s} \\ u_{msa} = \dfrac{u_{sa}}{U_s} \\ u_{mAn1} = \dfrac{u_{An1}}{U_s} \end{cases} \quad \begin{cases} u_{mo} = \dfrac{u_o}{U_s} \\ u_{Md} = \dfrac{U_d}{U_s}. \end{cases} \tag{25}$$

The current $U_s/\omega L_s$ is viewed as the reference value. The input current of the proposed rectifier i_a is expressed as

$$i_{ja} = \frac{\omega L_s}{U_s} i_a. \tag{26}$$

Substituting (7), (25), and (26) into (24) yields

$$u_{mLs} = \frac{di_{ja}}{d\varphi} = \sin(\varphi) - u_{mAn1} \tag{27}$$

where $\varphi = \omega t$.

From Fig. 5, Table I, and expression (27), the voltage u_{mLs} in interval $[\phi_2, \phi_2 + \pi]$ is expressed as (33) in the Appendix. From (33), the waveform of u_{mLs} can be charted, as shown in Fig. 7.

After normalization, the current i_{ja} meets

$$\begin{cases} i_{ja}(\varphi) = -i_{ja}(\varphi + \pi) \\ i_{ja}(\phi_2) = i_{ja}(\phi_2 + \pi) = 0. \end{cases} \tag{28}$$

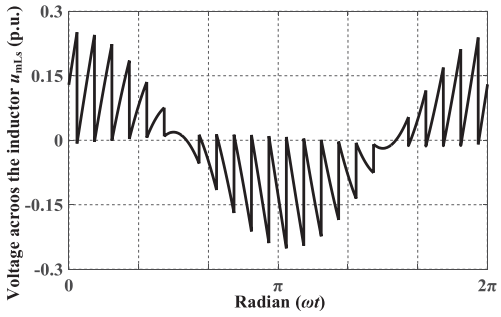

Fig. 7. Voltage across the inductor u_{mLs} after normalization.

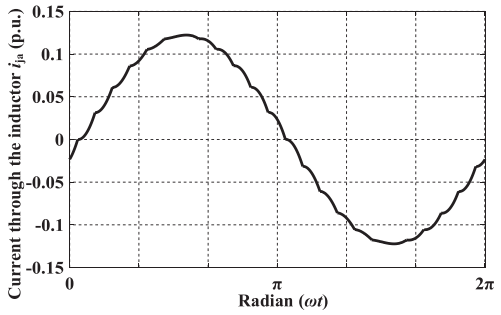

Fig. 8. Current i_{ja} after normalization.

Substituting (27) into (28) yields

$$\int_{\phi_2}^{\phi_2+\pi} [\sin(\varphi) - u_{mAn1}] d\varphi = 2\cos\phi_2 - \frac{\sqrt{3}\pi}{9}(u_{mo} + 4u_{Md}) = 0. \tag{29}$$

From (29), the phase difference ϕ_2 can be expressed as

$$\phi_2 = \arccos\frac{\pi}{6\sqrt{3}}(u_{mo} + 4u_{Md}). \tag{30}$$

From the range of ϕ_2 and expression (29), the load voltage u_{mo} should meet

$$u_{mo} \le \frac{6\sqrt{3}}{\pi} - 4u_{Md}. \tag{31}$$

From (27), Fig. 5, and Table I, the current i_{ja} in interval can be expressed as (34) in the Appendix.

From (34), the waveform of i_{ja} can be charted, as shown in Fig. 8. From Fig. 8, the current contains 24 arc lines per power supply cycle, which is close to sinusoidal wave.

In the proposed rectifier, the three input inductances are necessary. From Fig. 1, the relation among the power supply voltages (u_{sa}, u_{sb}, u_{sc}), the input voltages of the phase-shifting transformer (u_{An1}, u_{Bn1}, u_{Cn1}), and the voltages across the input inductances meets the Kirchhoff's voltage law. To set phase A as an example

$$u_{An1} = u_{sa} - u_{Ls} = u_{sa} - L\frac{di_a}{dt}. \tag{32}$$

In (32), u_{sa} is a known quantity. From (32), if the THD of the voltage u_{An1} is controlled to be minimal, the THD of the input current is minimal. The voltage u_{An1} is determined

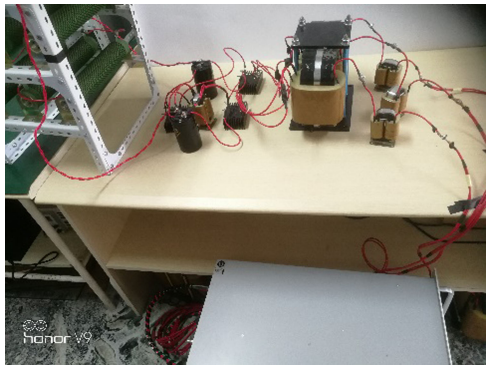

Fig. 9. Picture of the laboratory prototype.

by the injection transformer. When the injection transformer is designed optimally, the input voltages of the phase-shifting transformer (u_{An1}, u_{Bn1}, u_{Cn1}) contain 24 steps per power supply cycle, and the THD of the input voltages (u_{An1}, u_{Bn1}, u_{Cn1}) is about 7.6%. Due to the filtering of the input inductance, the THD of the input current is less than 7.6%.

IV. Experimental Validation

In this section, some related simulations and experiments are carried out based on a 1.7-kW rectifier system, which is built to validate the previous theoretical analysis. The simulation and experimental conditions are listed as follows: ① the three-phase input voltage is 220 V; ② the load resistance is 60 Ω; ③ the turn ratio of injection transformer is equal to 56; ④ the input inductance $L_s = 20$ mH; ⑤ the output capacitance $C_1 = C_2 = 3300$ μF/450 V; ⑥ the turn ratio of the Δ/Δ/Y isolated transformer meets $3\sqrt{3} : \sqrt{3} : 1$. Fig. 9 shows the picture of the laboratory prototype. The laboratory prototype includes three inductances, a phase-shifting transformer, two three-phase diode-bridge rectifiers, an injection transformer, two capacitors, and two diodes.

Fig. 10 shows the input voltages of the Δ/Δ/Y isolated transformer without the voltage harmonic injection circuit, and Fig. 11 shows the input voltages when using the circuit. In cases of without voltage harmonic injection circuit, input voltages have 12 steps per power supply cycle, whose theoretical and experimental values are around 15.2% and 9.74%. After using the voltage harmonic injection circuit, the step numbers of input voltages are doubled to 24 per power supply cycle, which leads to obvious reductions of THD both in theoretical and experimental values. The simulating result shows that THD declines to around 7.57% and that of experimental drops to 3.34%.

Fig. 12 shows the input currents of the isolated transformer without the voltage harmonic injection circuit, and Fig. 13 shows input currents of the proposed rectifier. When the voltage harmonic injection circuit is not used, the experimental THD value of the input currents is about 7.62%; after using the voltage harmonic injection circuit, the THD is about 2.65%. Due to the filtering of the input inductor L_s, the THD of the input currents is less than that of the input voltages.

From Figs. 10–13, there are some difference between the simulation results and the experimenting results. The leakage

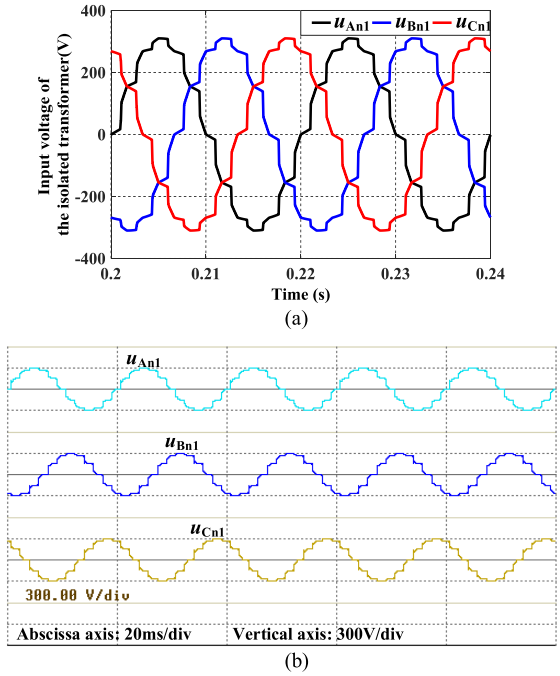

Fig. 10. Input voltages of the isolated transformer when not using the voltage harmonic injection circuit. (a) Simulation results. (b) Experimental results.

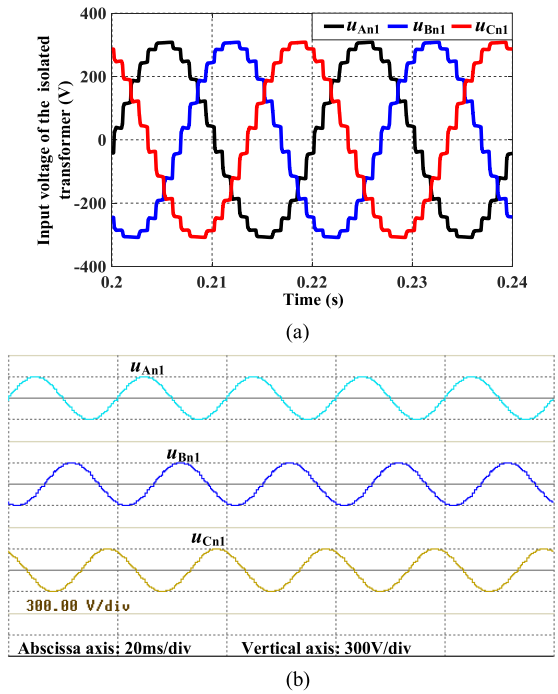

Fig. 11. Input voltage of the Δ/Δ/Y isolated transformer when using the voltage harmonic injection circuit. (a) Simulation results. (b) Experimenting results.

inductance of the phase-shifting transformer is ignored under simulation while that value cannot be ignored in experiments. Consequently, the THD of the input voltage and the input current in the experimenting results are less than that of the simulation results, at the same time, the waveforms of the input voltage and the input current in the experimenting results are smoother than that of the simulation results.

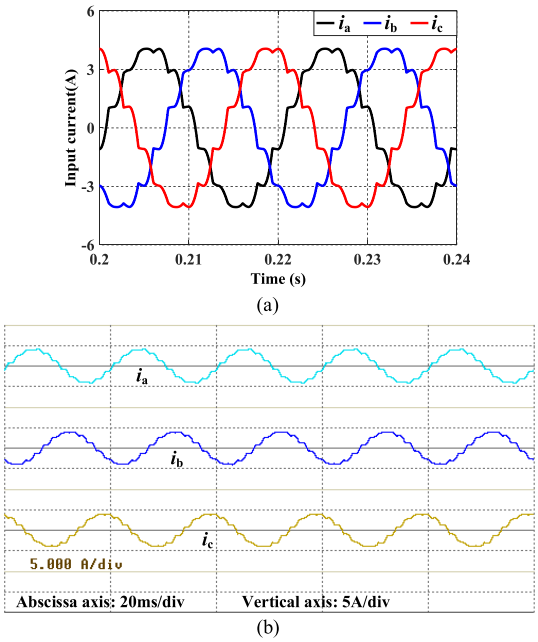

Fig. 12. Input currents of the 12-pulse rectifier when not using the hybrid voltage harmonic injection method. (a) Simulation results. (b) Experimental results.

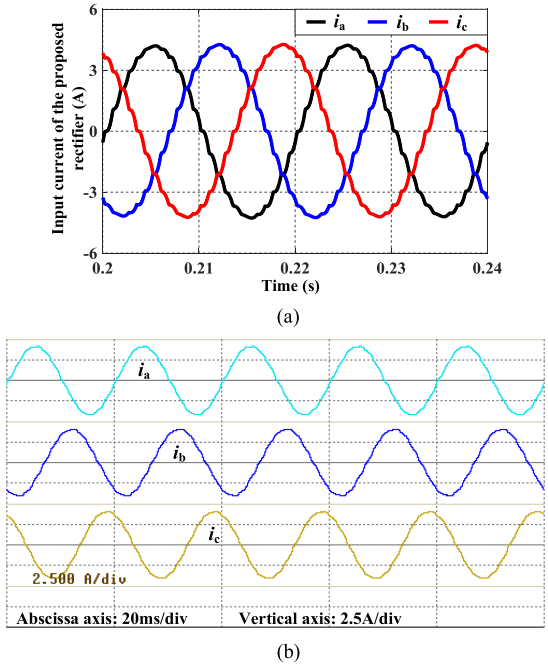

Fig. 13. Input currents of the proposed rectifier. (a) Simulation results. (b) Experimenting results.

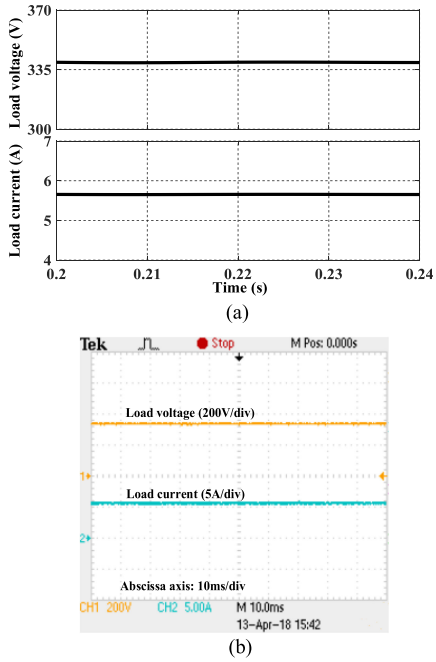

Fig. 14. Load voltage and load current. (a) Simulation results. (b) Experimenting results.

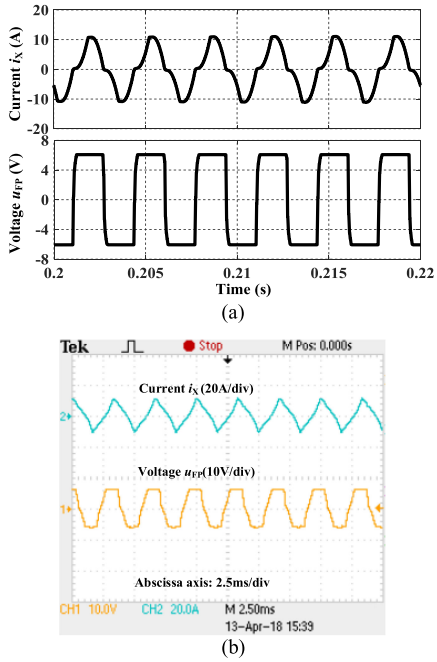

Fig. 15. Current through and voltage across the primary windings of the injection transformer. (a) Simulation results. (b) Experimental results.

Fig. 14 shows the load voltage and load current of simulations (a) and experiments (b). Under large capacitive load, the load voltage and load current are ripple free, thus the load can be equivalent to a constant-voltage load. The load voltage and load current are 328.6 and 5.48 A, respectively, and the load power is about 1800 W.

Fig. 15 shows the output current of the two three-phase diode-bridge rectifier and the voltage u_{FP} when using the hybrid voltage harmonic injection method. As shown in Fig. 15, the input currents of the isolated transformer are shaped, after using the voltage harmonic injection circuit, with the modulations of the output currents of two three-phase diode-bridge rectifiers.

Fig. 16 shows the output currents of the two three-phase diode-bridge rectifier after using the voltage harmonic injection circuit.

From Figs. 15 and 16, the current through the primary winding is $i_x = i_{Rec2} - i_{Rec1}$, and u_{FP} is a kind of square wave voltage whose frequency is six times of the supply frequency. The rms

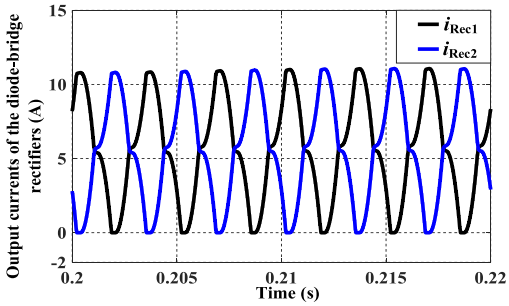

(a)

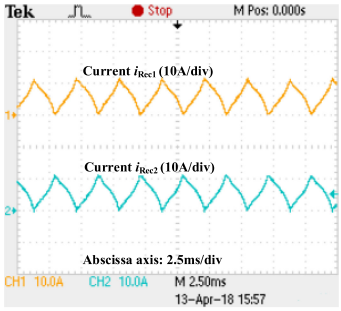

(b)

Fig. 16. Output currents of the two three-phase diode-bridge rectifiers. (a) Simulation results. (b) Experimental results.

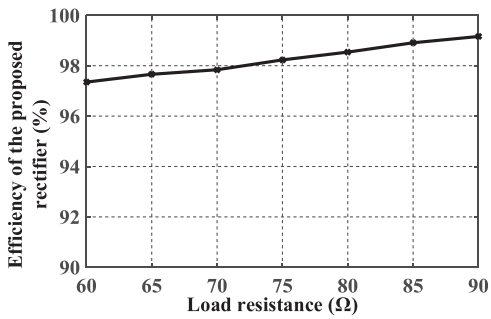

Fig. 17. Efficiency of the proposed rectifier when the load resistance varies.

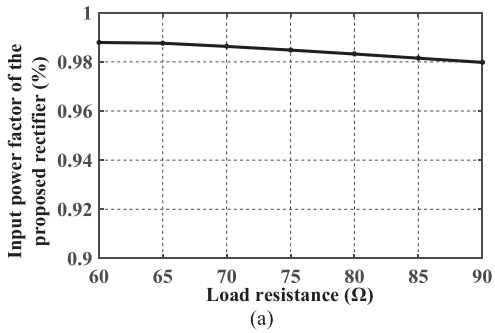

(a)

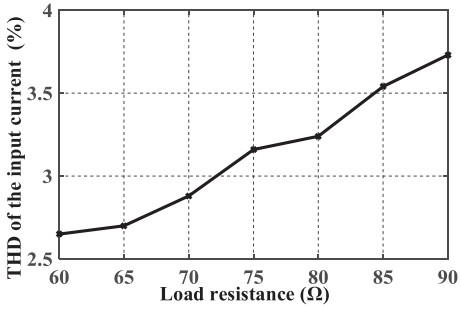

(b)

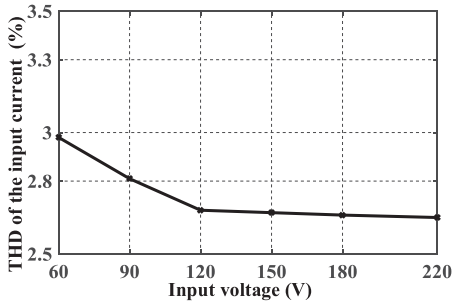

(c)

Fig. 18. Input power factor and THD of the input current. (a) Input power factor when the load resistance varies. (b) THD of the input current when the load resistance varies. (c) THD of the input current when the input voltage varies.

values of the current i_x and the voltage u_{FP} are 5.85 A and 5.868 V, respectively; the rms values of the current through and the voltage across the secondary winding are 73.98 mA and 328.6 V, respectively. It can be concluded that the kVA rating of the injection transformer is about 41.5W, which accounts for around 2.3% of the load power. Therefore, the cost of harmonic reduction is very low.

Fig. 17 shows the efficiency of the proposed rectifier when the rms value of the input voltages is equal to 220 V and load resistance varies from 60 to 90 Ω. From Fig. 17, the efficiency of the proposed rectifier shows a steady growth trend as the increase of the load resistance, which value rises from around 97.35% with the load resistance of 60 Ω to around 99.16% with the load resistance of 90 Ω. In general, the efficiency can be kept at about 98%.

When the rms value of the input voltages is equal to 220 V and load resistance varies from 60 to 90 Ω, Fig. 18(a) shows the input power factor of the proposed rectifier, and Fig. 18(b) shows the THD of the input current. The input power factor presents a slight downward trend from around 0.989 at the load resistance of 60 Ω to 0.98 at 90 Ω as shown in Fig. 18(a). However, a contrast tendency can be found in Fig. 18(b), the THD of the input current increases as the load resistance increases, which achieves the maximum value (about 3.73%) at 90 Ω. When the load resistance is a constant value of 60 Ω, Fig. 18(c) describes the THD variations of the input line current as increasing of the input voltage from 60 to 220 V, values of which are always below 3%.

Under unbalanced input voltage, the THD of the input line current is measured, as shown in Fig. 19. In Fig. 19, the input voltage rms values of phase a are equal to 206.8 (220 ∗ 94%) V, 211.2 (220 ∗ 96%) V, 215.6 (220 ∗ 98%) V, 220 (220 ∗ 100%) V, 224.4 (220 ∗ 102%) V, 228.8 (220 ∗ 104%) V, 233.2 (220 ∗ 106%) V, respectively; and the input voltage rms values of phases b and c are equal to 220 V. From Fig. 4, the changing trend of the THD becomes V shape; moreover, the THD increases with the increase of the unbalanced degree.

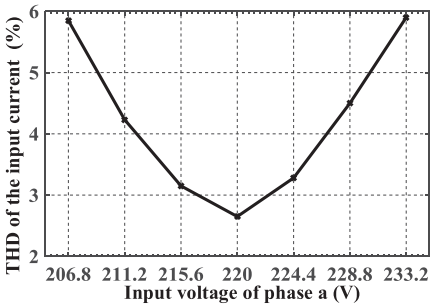

Fig. 19. THD of the input current under unbalanced input voltage. (For phase a, the rms value of the input voltage varies from 206.8 to 233.2 V; for phase b and c, the rms values of the input voltages are equal to 220 V).

V. Conclusion

This paper proposed a series-connected 24-pulse rectifier based on a passive voltage harmonic injection method, which uses an injection transformer and a single-phase bridge rectifier at the dc-link to generate injection voltage, then achieves the objective to reduce the harmonics of the input current. During one power supply cycle, the step number of input voltages of the phase-shifting transformer can be changed from 12 in a basic circuit to 24 in the proposed rectifier when the turn ratio of the injection transformer is optimally designed. The theoretical results demonstrated that the THD of the input voltage decreases from about 15.2% to 7.6% after using the proposed method. Due to the filtering of the input inductance, the theoretical THD of the input current is less than that of the input voltage regardless of using the proposed method. After using the proposed method, the experimental results show that the THD of the input line current is about 2.65%, which is less than that of the simulation results. Due to the presence of the leakage inductance of the phase-shifting transformer in experiments, which cannot be ignored as in simulations, the THD of the input voltage and current presented lower values in experimental results compared to that of simulations, that is, it can obtain more smoother input voltage and current waveforms in experiments. The harmonics of the input current are significantly reduced and the power factor is remarkably improved with the variations of the load resistance and input voltage; under unbalanced conditions, the proposed method can also reduce the harmonics effectively. The most notable point is that the cost of harmonic reduction will be quite low since the kVA rating of the injection transformer only takes around 2.3% of the load power. Moreover, the proposed rectifier is simple and easy to realize.

Appendix

$$u_{\mathrm{mLs}}(\varphi)=\begin{cases}\sin(\varphi)-\frac{2-\sqrt{3}}{2\sqrt{3}}\alpha_1+\frac{2+\sqrt{3}}{n\sqrt{3}}\alpha_2 & \varphi\in\left[\phi_2,\phi_2+\frac{\pi}{12}\right]\cup\left[\phi_2+\frac{11\pi}{12},\phi_2+\pi\right]\\ \sin(\varphi)-\frac{2-\sqrt{3}}{2\sqrt{3}}\alpha_1-\frac{2+\sqrt{3}}{n\sqrt{3}}\alpha_2 & \varphi\in\left[\phi_2+\frac{\pi}{12},\phi_2+\frac{\pi}{6}\right]\cup\left[\phi_2+\frac{5\pi}{6},\phi_2+\frac{11\pi}{12}\right]\\ \sin(\varphi)-\frac{\sqrt{3}-1}{2\sqrt{3}}\alpha_1+\frac{\sqrt{3}+1}{n\sqrt{3}}\alpha_2 & \varphi\in\left[\phi_2+\frac{\pi}{6},\phi_2+\frac{\pi}{4}\right]\cup\left[\phi_2+\frac{3\pi}{4},\phi_2+\frac{5\pi}{6}\right]\\ \sin(\varphi)-\frac{\sqrt{3}-1}{2\sqrt{3}}\alpha_1-\frac{\sqrt{3}+1}{n\sqrt{3}}\alpha_2 & \varphi\in\left[\phi_2+\frac{\pi}{4},\phi_2+\frac{\pi}{3}\right]\cup\left[\phi_2+\frac{2\pi}{3},\phi_2+\frac{3\pi}{4}\right]\\ \sin(\varphi)-\frac{1}{2\sqrt{3}}\alpha_1+\frac{1}{n\sqrt{3}}\alpha_2 & \varphi\in\left[\phi_2+\frac{\pi}{3},\phi_2+\frac{5\pi}{12}\right]\cup\left[\phi_2+\frac{7\pi}{12},\phi_2+\frac{2\pi}{3}\right]\\ \sin(\varphi)-\frac{1}{2\sqrt{3}}\alpha_1-\frac{1}{n\sqrt{3}}\alpha_2 & \varphi\in\left[\phi_2+\frac{5\pi}{12},\phi_2+\frac{7\pi}{12}\right]\end{cases}\tag{33}$$

where $\alpha_1=u_{mo}+4u_{Md}$, $\alpha_2=u_{mo}+u_{Md}$, and ϕ_2 is the phase difference between i_{ja} and u_{mLs}

$$i_{ja}(\varphi)=\begin{cases}\alpha_3-\alpha_4+\frac{\pi\alpha_1}{6\sqrt{3}}-\cos(\varphi) & \varphi\in\left[\phi_2,\phi_2+\frac{\pi}{12}\right]\\ \alpha_3+\alpha_4+\frac{\pi\alpha_1}{6\sqrt{3}}+\frac{2+\sqrt{3}}{n6\sqrt{3}}\pi\alpha_2-\cos(\varphi) & \varphi\in\left[\phi_2+\frac{\pi}{12},\phi_2+\frac{\pi}{6}\right]\\ \alpha_5-\alpha_6+\frac{2\sqrt{3}-1}{12\sqrt{3}}\pi\alpha_1-\frac{\sqrt{3}+1}{n6\sqrt{3}}\pi\alpha_2-\cos(\varphi) & \varphi\in\left[\phi_2+\frac{\pi}{6},\phi_2+\frac{\pi}{4}\right]\\ \alpha_5+\alpha_6+\frac{2\sqrt{3}-1}{12\sqrt{3}}\pi\alpha_1+\frac{\sqrt{3}+1}{n3\sqrt{3}}\pi\alpha_2-\cos(\varphi) & \varphi\in\left[\phi_2+\frac{\pi}{4},\phi_2+\frac{\pi}{3}\right]\\ \alpha_7-\alpha_8+\frac{\pi\alpha_1}{4\sqrt{3}}-\frac{\pi\alpha_2}{n3\sqrt{3}}-\cos(\varphi) & \varphi\in\left[\phi_2+\frac{\pi}{3},\phi_2+\frac{5\pi}{12}\right]\\ \alpha_7+\alpha_8+\frac{\pi\alpha_1}{4\sqrt{3}}+\frac{\pi\alpha_2}{n2\sqrt{3}}-\cos(\varphi) & \varphi\in\left[\phi_2+\frac{5\pi}{12},\phi_2+\frac{7\pi}{12}\right]\\ \alpha_7-\alpha_8+\frac{\pi\alpha_1}{4\sqrt{3}}-\frac{2\pi\alpha_2}{n3\sqrt{3}}-\cos(\varphi) & \varphi\in\left[\phi_2+\frac{7\pi}{12},\phi_2+\frac{2\pi}{3}\right]\\ \alpha_5+\alpha_6+\frac{4\sqrt{3}-5}{12\sqrt{3}}\pi\alpha_1+\frac{2\sqrt{3}+2}{n3\sqrt{3}}\pi\alpha_2-\cos(\varphi) & \varphi\in\left[\phi_2+\frac{2\pi}{3},\phi_2+\frac{3\pi}{4}\right]\\ \alpha_5-\alpha_6+\frac{4\sqrt{3}-5}{12\sqrt{3}}\pi\alpha_1-\frac{5\sqrt{3}+5}{n6\sqrt{3}}\pi\alpha_2-\cos(\varphi) & \varphi\in\left[\phi_2+\frac{3\pi}{4},\phi_2+\frac{5\pi}{6}\right]\\ \alpha_3+\alpha_4+\frac{5-3\sqrt{3}}{6\sqrt{3}}\pi\alpha_1+\frac{10+5\sqrt{3}}{n6\sqrt{3}}\pi\alpha_2-\cos(\varphi) & \varphi\in\left[\phi_2+\frac{5\pi}{6},\phi_2+\frac{11\pi}{12}\right]\\ \alpha_3-\alpha_4+\frac{5-3\sqrt{3}}{6\sqrt{3}}\pi\alpha_1-\frac{2+\sqrt{3}}{n\sqrt{3}}\pi\alpha_2-\cos(\varphi) & \varphi\in\left[\phi_2+\frac{11\pi}{12},\phi_2+\pi\right]\end{cases}\tag{34}$$

where

$$\begin{cases}\alpha_3=\frac{2-\sqrt{3}}{2\sqrt{3}}(u_{mo}+4u_{Md})(\phi_2-\varphi)\\ \alpha_4=\frac{2+\sqrt{3}}{n\sqrt{3}}(u_{mo}+u_{Md})(\phi_2-\varphi)\\ \alpha_5=\frac{\sqrt{3}-1}{2\sqrt{3}}(u_{mo}+4u_{Md})(\phi_2-\varphi)\end{cases}\quad\begin{cases}\alpha_6=\frac{\sqrt{3}+1}{n\sqrt{3}}(u_{mo}+u_{Md})(\phi_2-\varphi)\\ \alpha_7=\frac{u_{mo}+4u_{Md}}{2\sqrt{3}}(\phi_2-\varphi)\\ \alpha_8=\frac{u_{mo}+u_{Md}}{n\sqrt{3}}(\phi_2-\varphi).\end{cases}\tag{35}$$

REFERENCES

[1] B. Singh, S. Gairola, B. N. Singh, A. Chandra, and K. Al-Haddad, "Multipulse AC–DC converters for improving power quality: A review," *IEEE Trans. Power Electron.*, vol. 23, no. 1, pp. 260–281, Jan. 2008.

[2] J. Sun, Z. Bing, and K. J. Karimi, "Input impedance modeling of multipulse rectifiers by harmonic linearization," *IEEE Trans. Power Electron.*, vol. 24, no. 12, pp. 2812–2820, Dec. 2009.

[3] Q. Pan, W. Ma, D. Liu, Z. Zhao, and J. Meng, "A new critical formula and mathematical model of double-tap interphase reactor in a six-phase tap-changer diode rectifier," *IEEE Trans. Ind. Electron.*, vol. 54, no. 1, pp. 479–485, Feb. 2007.

[4] Y. Shiyan, M. Fangang, and Y. Wei, "Optimum design of inter-phase reactor with double-tap-changer applied to multi-pulse diode rectifier," *IEEE Trans. Ind. Electron.*, vol. 57, no. 9, pp. 3022–3029, Sep. 2010.

[5] S. Choi, B. S. Lee, and P. N. Enjeti, "New 24-pulse diode rectifier systems for utility interface of high power AC motor drives," *IEEE Trans. Ind. Appl.*, vol. 33, no. 2, pp. 531–541, Mar./Apr. 1997.

[6] F. Meng, W. Yang, S. Yang, and L. Gao, "Active harmonic reduction for 12-pulse diode bridge rectifier at DC side with two-stage auxiliary circuit," *IEEE Trans. Ind. Informat.*, vol. 11, no. 1, pp. 64–73, Feb. 2015.

[7] B. S. Lee, J. Hahn, and P. N. Enjeti, "A robust three-phase active power factor correction and harmonic reduction scheme for high power," *IEEE Trans. Ind. Electron.*, vol. 46, no. 3, pp. 483–494, Jun. 1999.

[8] S. Choi, P. N. Enjeti, H. H. Lee, and I. J. Pitel, "A new active interphase reactor for 12-pulse rectifiers provides clean power utility interface," *IEEE Trans. Ind. Appl.*, vol. 32, no. 6, pp. 1304–1311, Nov./Dec. 1996.

[9] H. Akagi and K. Isozaki, "A hybrid active filter for a three-phase 12-pulse diode rectifier used as the front end of a medium-voltage motor drive," *IEEE Trans. Power Electron.*, vol. 27, no. 1, pp. 69–77, Jan. 2012.

[10] I. Araujo-Vargas, A. J. Forsyth, and F. Javier Chivite-Zabalza, "High-Performance multipulse rectifier with single-transistor active injection," *IEEE Trans. Power Electron.*, vol. 23, no. 3, pp. 1299–1308, Mar. 2008

[11] S. Fukuda, M. Ohta, and Y. Iwaji, "An auxiliary-supply-assisted harmonic reduction scheme for 12-pulse diode rectifiers," *IEEE Trans. Power Electron.*, vol. 23, no. 3, pp. 1270–1277, Mar. 2008.

[12] F. Javier Chivite-Zabalza and A. J. F. D. R. Trainer, "A simple, passive 24-pulse AC-DC converter with inherent load balancing," *IEEE Trans. Power Electron.*, vol. 21, no. 2, pp. 430–439, Feb. 2006.

Fangang Meng (M'15) was born in Shandong, China, in 1982. He received the B.S. degree in thermal energy and power engineering in 2005, and the M.S. and Ph.D. degrees in electrical engineering in 2007 and 2011, respectively, from Harbin Institute of Technology, Harbin, China.

Since 2011, he has been working as an Assistant Professor with the Harbin Institute of Technology.

His research interests include harmonic detection, stability analysis of converters, and high power rectification.

Qingxiao Du was born in Shandong, China, in 1995. She received the B.S. degree in electrical engineering from the Harbin Institute of Technology, Weihai, Weihai, China, in 2017, and the M.S. degree in electrical power engineering from the University of Southampton, Southampton, U.K., in 2018.

Her current research interests include multi-pulse rectifier and power electronic transformer.

Lin Wang was born in Zhejiang, China, in 1993. She received the B.S. degree in electrical engineering in 2016 from the Harbin Institute of Technology, Weihai, Weihai, China, where she has been working toward the M.S. degree in power electronics and power drives since 2016.

Her research interests include multi-pulse rectifier, power electronic transformer, and high-power rectification.

Lei Gao was born in Hebei, China, in 1982. She received the B.S. degree, M.S. degree, and Ph.D. degrees in electrical engineering from Harbin Institute of Technology, Harbin, China, in 2005, 2007, and 2012, respectively. Since 2012, she has been a Lecturer with Harbin Institute of technology.

Her current research interests include power electronics and motor drives.

Zhongcheng Man was born in Shandong, China, in 1993. He received the B.S. degree in electrical engineering in 2017 from China University of Mining and Technology, Xuzhou, China. Since 2017, he has been working toward the M.S. degree in power electronics and power drives with Harbin Institute of Technology, Weihai, China.

His research interests include multi-pulse rectifiers, power electronic transformers, and high-power rectification.